ACS Partner Journal
ACCOUNTS of materials research
pubs.acs.org/amrcda
Article

Interfacial Solar Vapor Generation: Materials and Structural Design

Xinzhe Min,† Bin Zhu,† Bo Li,† Jinlei Li, and Jia Zhu*

Cite This: https://dx.doi.org/10.1021/accountsmr.0c00104

CONSPECTUS: The global water scarcity and deteriorating environment call for the development of environmentally friendly water treatment technologies. Solar-driven evaporation, well-known as a critical step of water cycles, provides a natural inspiration for water treatment and purification with a minimized carbon footprint. The emergence of interfacial solar vapor generation enabled through carefully tailored materials design in recent years offers an effective approach to enhance solar evaporation, with unique thermodynamic and kinetic advantages. Thermodynamically, by localizing absorbed solar energy at the water surface to avoid thermal dissipation into the entire body of water, high solar vapor transfer efficiency can be achieved. Kinetically, because of reduced thermal mass, a short response time of vapor generation and fast ramping of vapor temperature can be expected.

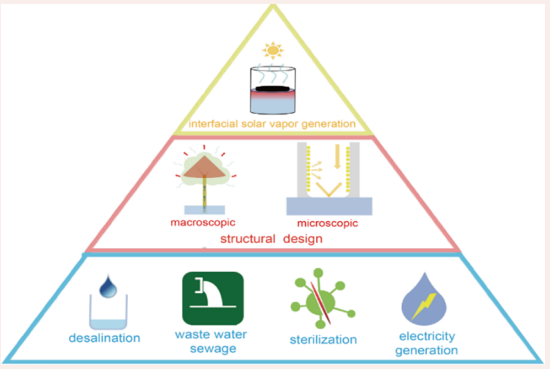

In this perspective review, we start by exhibiting the structural designs of interfacial solar vapor generators to improve the energy transfer efficiency and evaporation rate: first, tuning optical structures to improve the light absorption; second, designing a two-dimensional water path and bioinspired structures to reduce the heat loss; third, harvesting environmental energy as an extra energy input to further increase the evaporation rate. Then, we demonstrate the intrinsic thermodynamic and kinetic advantages of interfacial solar evaporation for various applications. On the thermodynamic side, low energy loss and a high evaporation rate enable effective desalination and water treatment. While on the kinetic side, quick-response and high-temperature steam generation has direct implications in fields like sterilization and power generation. In the end, we briefly conclude the main challenges in fundamental and technical aspects as well as discuss various promising pathways for future development.

1. INTRODUCTION

Solar energy and water are among the most abundant resources on earth. Solar evaporation, the phase transition from water to vapor powered by solar energy, is a critical component of natural water cycles. Through this process, vapor or steam, as a useful form of energy, is generated while solute in the water is left behind, leading to separation of water and solute. Therefore, solar evaporation can have direct implications in a broad range of applications, such as desalination, sterilization, power generation, and wastewater treatment. For industrial usages, a high energy transfer efficiency and evaporation rate are indispensable.[1−3] Several heating methods has been proposed to avoid the radiation, convection, and conduction heat loss and to enhance the efficiency in practical applications.[4−7] Among all of these approaches, solar-driven interfacial vapor generation is recently emerging as a most promising pathway to effectively increase the energy transfer efficiency.[8−14]

Intrinsically, water evaporation is a surface-dominated process, in which the phase transition mostly occurs at the air−water interface, which implies that the surface energy localization should be beneficial. Typically, during interfacial solar vapor generation, a tailored evaporator is floating on the surface of the water source. Under sunlight illumination, the evaporator will absorb the solar energy efficiently and transfer the energy to a thin layer of water in close proximity instead of the entire bulk water, to induce a direct liquid−vapor transition (Figure 1A). Therefore, the efficiency of interfacial solar vapor generation will not be affected by the difference of bulk water's volume, which exhibits great potential in large-scale industrial applications.[15]

The solar vapor transfer efficiency (η), defined as the ratio of the energy consumed for evaporation (P_{eva}) to the total input solar energy(P_{solar}) (seen in eq 1), is a vital parameter to evaluate the performance of an interfacial solar evaporation system.[3]

$$\eta = P_{eva}/P_{solar} \quad (1)$$

$$P_{eva} = P_{solar}{}^{*}\alpha - (P_{ra} + P_{cd} + P_{cv}) \quad (2)$$

Received: December 11, 2020
Revised: February 10, 2021

https://dx.doi.org/10.1021/accountsmr.0c00104
Acc. Mater. Res. XXXX, XXX, XXX−XXX

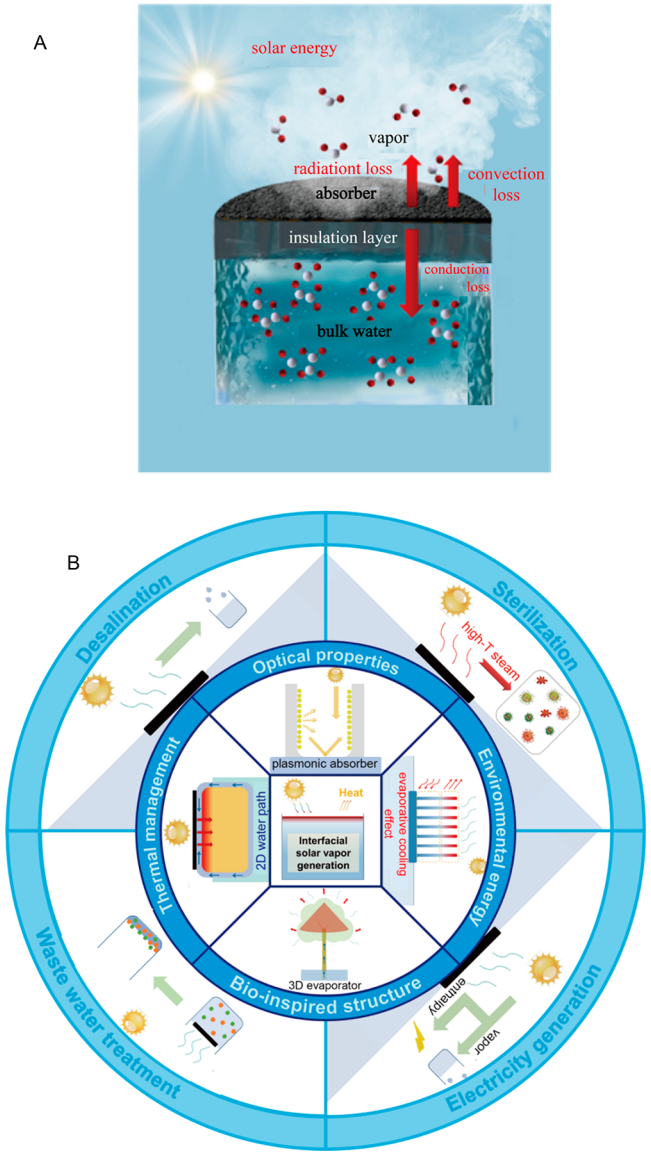

Figure 1. (A) Schematic of interfacial solar vapor generation and energy flow. (B) Schematic view of this Article: structures, devices, and applications of interfacial solar vapor generation.

In eq 2, P_{eva} represents the energy consumed for water evaporation, P_{solar} denotes the total energy of solar light input, and α represents the absorptivity of the absorber. $P_{ra} + P_{cd} + P_{cv}$ stands for the total heat loss of the system, which mainly depends on the temperature of evaporation and can be described as three different components: radiation loss (P_{ra}), convection loss (P_{cv}), and conduction loss (P_{cd}). It is clear that maximizing absorption as well as minimizing total heat loss are critical to enable a high efficiency.

Previous reviews have covered the exciting progress of interfacial solar vapor generation so far.[16−22] This account provides a systematical analysis and summary from the perspective of kinetics and thermodynamics for interfacial solar vapor generation. In this perspective review, we start by exhibiting the structural designs of interfacial solar vapor generators to improve the thermodynamic energy transfer efficiency and evaporation rate: first, tuning optical structures to improve the light absorption; second, designing a two-dimensional water path and bioinspired structures to reduce the heat loss; third, harvesting environmental energy as an extra energy input to further increase the evaporation rate (Figure 1B). We also reveal the kinetic advantage of interfacial solar vapor generation as a result of a reduced thermal mass in interfacial-type heating. Based on the thermodynamic and kinetic advantages, we further present a few examples of devices and related applications based on interfacial solar vapor generation, including desalination, wastewater treatment, sterilization, and electricity generation (Figure 1B).

2. PERFORMANCES OF SOLAR VAPOR GENERATION

For sustainable development of solar vapor generations, it is important to evaluate the performance. As solar vapor generations have direct implications in various fields, specific applications dictate the figures of merit. For applications related to the separation of water and solute, such as desalination and wastewater treatment, the evaporation rate and solar vapor energy transfer efficiency are important.[23] For applications that require a high steam temperature and fast response time, for example, solar steam sterilization, the response time and temperature of the generated steam are also considered as the two most important parameters. At present, several aspects of structural designs, including the optical and thermal management and structural designs of the evaporators, have been investigated to achieve a high solar vapor energy transfer efficiency, high steam temperature, and fast response time.

2.1. Thermodynamic Aspect: Energy Transfer Efficiency and Evaporation Rate

2.1.1. Tailoring Nanostructures for Broadband and Efficient Light Absorption. Broadband and efficient light absorption is the first and foundational step for solar vapor generation processes. Various materials possess high solar absorption, with great potential as effective solar absorbers.[13−15,24−32] Among all of these materials, three kinds of solar absorbers, namely carbon-based, semiconductor-based, and plasmonic-based absorbers, have been widely investigated in recent years. Table 1 lists some typical examples.

Table 1. Comparison of Different Solar Absorbers in Terms of Light Absorption and Cost

materials	category	absorption (%)	cost ($/kg)	ref
GO membrane	carbon	94	<10	15
carbonized mushroom	carbon	95	<10	17
TiO_2 particles	semiconductor	97	<50	18
Au nanoparticles	plasmonic	99	>650	13
Al nanoparticles	plasmonic	95	<10	14

Carbon-based solar absorbers, including graphite, reduced graphene oxides, and carbonized organic compounds, naturally possess high solar absorption. During the light absorbing process, the optically excited electrons can be thermalized to realize effective heat generation. While for semiconductor-based solar absorbers, their high absorption mainly relies on their intrinsic optical properties. The excited high-energy photoelectrons release their energy during the relaxation to realize the effective heating effect, which makes carbon-based solar absorbers a promising material for solar vapor generation.

Among various absorbers developed, plasmonic solar absorbers have also attracted intensive attention[33,34] due to their broadband light response and flexible spectral manipu-

https://dx.doi.org/10.1021/accountsmr.0c00104
Acc. Mater. Res. XXXX, XXX, XXX−XXX

lation.[35] Through two mechanisms, (1) surface plasmon polaritons (SPPs) and (2) localized surface plasmons (LSPs),[36,37] these plasmonic absorbers harvest solar energy and redistribute it into heat via the electron−electron and electron−phonon scattering processes.

Noble-metal plasmonic materials with high electron concentrations, such as gold and silver, are considered as ideal candidates for constructing plasmonic absorbers due to their strong plasmonic response in the visible and infrared (IR) region, matching well with solar spectral irradiance. However, as most of the plasmonic building blocks only respond to a certain wavelength range rather than covering the entire solar spectrum, it is crucial to tailoring and assembling the nanostructures of plasmsonic absorbers. In 2016, Zhou et al. reported a plasmonic absorber fabricated by assembling gold NPs onto a three-dimensional nanoporous alumina template through a one-step deposition process[13] (Figure 2A). This plasmonic absorber

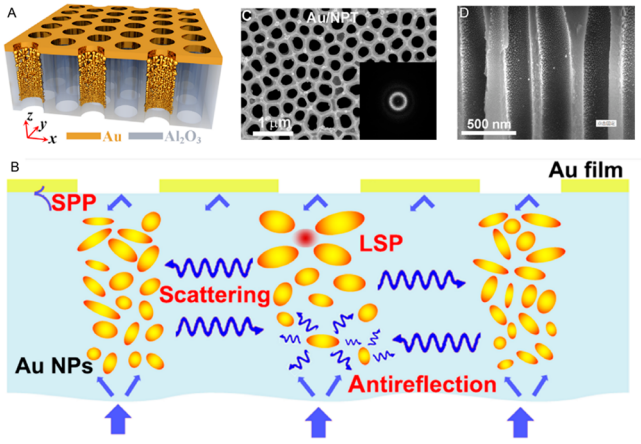

Figure 2. (A) Schematic of Au-based plasmonic absorbers self-assembled on a three-dimensional porous template. (B) Physical mechanisms of Au-NP-based broadband plasmonic absorbers. (C,D) Top view (C) and cross-sectional (D) SEM images of a Au-NP-based plasmonic absorber. Reproduced with permission from ref 13. Copyright 2016 The American Association for the Advancement of Science.

developed enables broadband and effective absorption solar energy (~99%, weighted by AM1.5G solar spectrum) for three reasons (Figure 2B): (1) A high density of plasmonic modes, beneficial for broadband solar absorption, are formed by self-assembly of close-packed gold NPs into three-dimensional porous templates (Figure 2B). (2) The three-dimensional porous template provides channels for multiple avenues of internal scattering of light without wavelength selectivity and thus greatly enhances the absorption path length. (3) The entire structure possesses a high porosity as well as a low metal filling ratio, which results in a rather low effective refractive index and thus greatly decreases the optical loss of surface reflectance.

Aluminum, with a plasmonic response in the ultraviolet (UV) region and a relatively low cost ($1000 per ton) compared with silver and gold, is promising for building a cost-effective plasmonic absorber. Zhou et al. reported an alumina-based solar absorber, consisting of close-packed aluminum NPs and a thin layer of anodic oxidized aluminum film, produced by an all-aluminum-based process.[14] Besides the strong intrinsic interband absorption of aluminum at ~800 nm, another key feature of the aluminum-based plasmonic absorber is that it has a self-limiting oxide layer, which further promotes the overall absorption performance and enhances its stability. As a result, the reported aluminum-based plasmonic absorber demonstrated an effective absorption efficiency of >95% from 400 to 2500 nm (weighted by standard solar irradiance AM 1.5G), and the solar-to-vapor efficiency reached ~ 90% under an illumination of 4 kW/m^2.

2.1.2. 2D Water Path for Reducing Conduction Heat Loss. Besides broadband and efficient solar absorption, heat losses (conduction P_{cd}, radiation P_{ra}, and convection P_{cv}) during the evaporation process also need to be addressed for further improving the solar-to-vapor conversion efficiency.

The conduction heat loss P_{cd} is caused by the temperature gradient between the high-temperature surface of the absorber (T_1) and the low-temperature bulk water (T_2), as shown in eq 3, where $\frac{k}{L}$ represents the thermal conductivity between bulk water and the absorber. As a result, it is expected that materials of low thermal conductivity are ideal to serve as a thermal insulation layer to realize heat localization.

$$P_{cd} = k\left(\frac{T_1 - T_2}{L}\right) \tag{3}$$

In this regard, GO-based aerogels (GO-SA-CNT aerogels) with high porosity and low thermal conductivity were fabricated to enable efficient solar vapor generation.[38] The highly porous structure endows these GO-based aerogels with low density (1.2−17.6 mg/cm^3) as well as low thermal conductivity (<0.05 W/mK), while the porous structure also ensures a sufficient water supply for evaporation.

Later on, it is realized that even for evaporators with low thermal conductivity, water in direct contact can still carry heat flow away. To address this issue, confined water supply paths, such as one-dimensional (1D) and two-dimensional (2D) water paths, were proposed to further suppress conduction heat loss while maintaining a sufficient water supply.[15] A thermal insulator with a 0.04 W/mK thermal conductivity is used to suppress conduction heat loss, while cellulose coating on the surface serves as the confined water path (Figure 3A). As a result, an evaporation rate of 1.45 kg/m^2 h and an energy transfer efficiency of approximately 80% can be achieved (Figure 3B). Most importantly, because of suppressed heat conduction loss, the achieved energy transfer efficiency is independent of water volume. The authors built two devices with and without a 2D water path respectively to test their performance with different water quantities (Figure 3C). As we can see from Figure 3D,E, a device based on a 2D water path possesses obvious thermodynamic advantages; the evaporation rate of it remains stable while the bulk-heating-based device shows a decreasing evaporation rate as the water volume increases. The volume-independence of the devices with 2D water path not only lays down a solid foundation for large-scale application but also represents the most important signature of "interfacial-type" solar evaporation.

2.1.3. Bioinspired Structural Design for Suppressing Convection and Radiation Losses. With a well-designed water path, conduction heat loss can be effectively suppressed. However, based on eq 2, a further increase of the solar-to-vapor conversion efficiency requires suppression of the convection and radiation heat losses.

Convection heat loss as well as radiation heat loss mostly depends on the surface temperature of the evaporator, as described in eqs 4 and 5, where T_3 and T_4 represent the temperature of the evaporator and ambient, respectively, ε

https://dx.doi.org/10.1021/accountsmr.0c00104
Acc. Mater. Res. XXXX, XXX, XXX−XXX

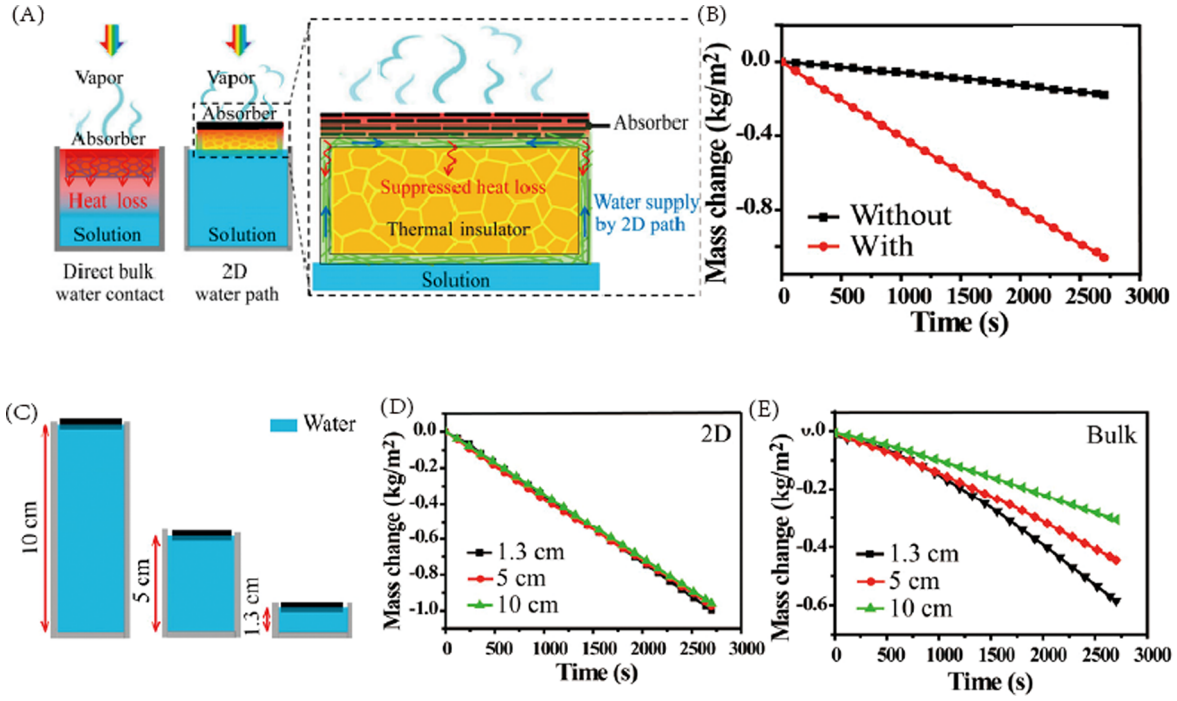

Figure 3. (A) Schematics of conventional solar vapor generation with direct water contact, and schematics of solar desalination devices with suppressed heat loss and a 2D water supply. (B) Mass changes over time with and without samples with a 2D water path. (C) Schematics of devices using beakers with the same diameter (~2.6 cm) but different water heights; 1.3, 5, and 10 cm in height correspond to 7, 26.5, and 53 mL in volume, respectively. (D) Mass changes over time with the 2D water path device using different water quantities. (E) Mass changes over time with the direct bulk water contact device using different water quantities. Reproduced with permission from ref 15. Copyright 2016 National Academy of Sciences.

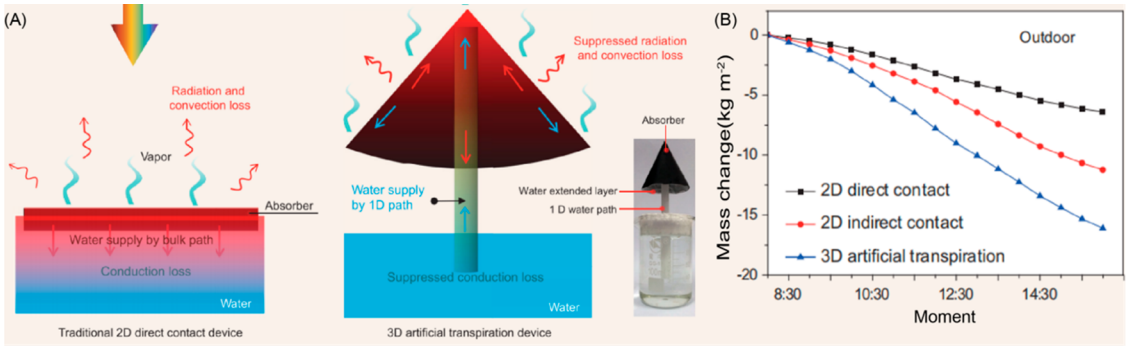

Figure 4. (A) Schematics of a conventional solar evaporator with direct water contact (2D direct conduct), and schematics of the 3D artificial transpiration device with suppressed heat loss. (B) Mass changes over time outdoors using the 2D direct contact evaporator, 2D indirect contact evaporator, and 3D artificial transpiration device, respectively. Reproduced with permission from ref 40. Copyright 2018 Oxford University Press.

denotes the emissivity, and h stands for the convective heat transfer coefficient.

$$q_{ra} = \sigma\varepsilon(T_3^4 - T_4^4) \quad (4)$$

$$q_{cv} = h(T_3 - T_4) \quad (5)$$

Therefore, one rational strategy to decrease the surface temperature of the evaporator is to increase its effective evaporation area. Bioinspired structures, such as a mushroom structure or a tree-like structure, are ideal for this purpose, as they are capable of both maximizing the evaporation area and providing excellent water transportation through a confined pathway.[39]

In 2017, a 3D artificial transpiration evaporator[40] was reported, which contains two main parts: (1) the upper absorber, which has the shape of the crown of a tree, and (2) the bottom trunk-like 1D water path, as shown in Figure 4A. The evaporator with such a unique structure maximizes the evaporative surface area, which not only ensures sufficient evaporation but also decreases the average power input per unit area, therefore leading to a decreased surface temperature, suppressing losses of radiation and convection, compared to the conventional design. Also, a 1D water path design ensures a water supply as well as suppressed heat conduction loss. As a result, the solar vapor transfer efficiency can reach up to 85% under 1 sun of illumination, without any external thermal insulation and optical support system (Figure 4B).

It is also interesting to reveal that natural mushrooms without any processing can achieve 68% energy transfer efficiency because of an umbrella-like structure and 1D water supply.[17] After a carbonization process, the solar-to-vapor energy transfer efficiency further increases to 78% because of enhanced absorption during carbonization. In addition, other evaporators

https://dx.doi.org/10.1021/accountsmr.0c00104
Acc. Mater. Res. XXXX, XXX, XXX−XXX

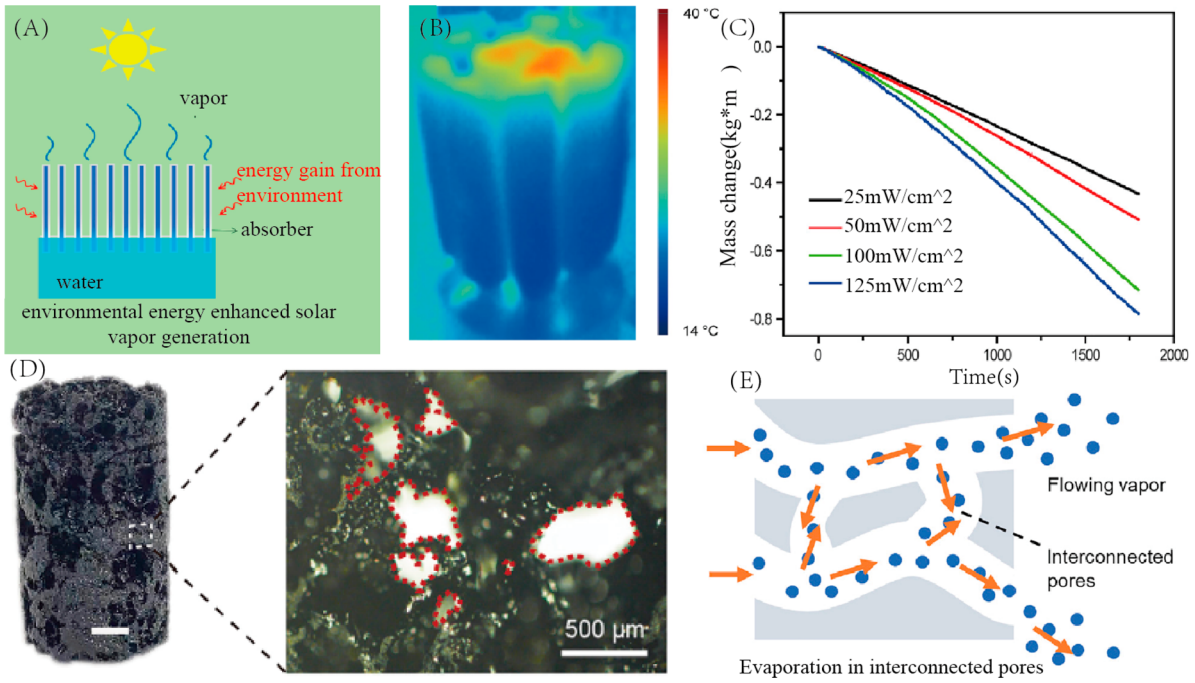

Figure 5. (A) For the environmental-energy-enhanced interfacial solar vapor generator, a net energy gain from the environment leads to an evaporation rate exceeding the value assuming a 100% solar-to-vapor energy transfer efficiency. (B) Infrared images of the environmental-energy-enhanced interfacial solar vapor generator under 100 mW/cm^2. (C) The mass changes of water with the environmental-energy-enhanced interfacial solar vapor generator over time under different light intensities. (D) A photograph of the 3D interconnected porous carbon foam (scale bar, 1 cm) and a optical micrograph of the 3D IPCF. The sizes of these interconnected pores range from a few tens of micrometers to a few millimeters. (E) A schematic of effective evaporation enabled by interconnected pores. The interconnected porous structure allows effective diffusion of vapor with a convective flow. Reproduced with permission from ref 43. Copyright 2018 Elsevier.

based on biomass charcoal with intrinsic structural properties such as wood and tree leaf charcoal also demonstrated high energy efficiency and evaporation rate.[41,42]

2.1.4. Environmental-Energy-Enhanced Solar Evaporation. Assuming a standard solar irradiance (1000 W/m^2, AM1.5G), a fixed enthalpy of evaporation, and minimized optical and thermal losses, it is natural to estimate that the evaporation rate of a typical interfacial solar evaporating system has a upper limit around 1.47 kg/m^2 h, hindering further development of an interfacial solar-vapor-generation technique for more industrial applications. However, pursuing a higher evaporation rate would require convenient utilization of an additional energy source such as environmental energy and wind energy, which is considered a main challenge nowadays.

To overcome this challenge, several novel solutions have been proposed by researchers. As an example, in 2018, Zhu's group demonstrated a three-dimensional evaporator, which can not only harvest solar energy but also utilize environmental energy.[43] The key to achieve a net energy input from the environment is to cool down the evaporative surface of evaporators below the environmental temperature. As shown in Figure 5A, in this three-dimensional evaporator, while the temperature of the top surface is higher than the environmental temperature because of strong light absorption, the temperature of the sidewall of the evaporators is lower than the environmental temperature because of the effect of evaporative cooling (Figure 5B). Because of a net energy gain from the environment, an evaporation rate of 1.62 kg/m^2 h under 1 sun is achieved, which is above the assumed evaporation rate (1.47 kg/m^2 h) (Figure 5C). There are several other designs to achieve environmental-energy-enhanced evaporation, which together provide a promising strategy for further increasing the evaporation rate.[40,44]

As we know, the performance of solar absorbers is highly dependent on the evaporative surface and vapor diffusion. However, for a typical porous solar absorber, vapor will be confined instead of diffusing out due to the close ends of porous structure, which greatly restricts the evaporation rate. In 2020, Li et al. demonstrated a carbon foam with an interconnected porous structure as a solar evaporator (Figure 5D).[45] The carbon foam can obtain wind energy as an additional energy source due to its interconnected porosity, which allows the utilization of convective flow to ensure effective vapor diffusion (Figure 5E). As the performance of the carbon foam is highly related with its porosity, the authors tested several samples with different pore sizes. With the pore size of 5.8 mm and convective flow of 6 m/s, a remarkable evaporation rate of 10.9 kg/m^2 h is achieved, which is an order of magnitude above previous work, showing great potential in practical applications.

2.2. Kinetic Aspect: Response Time

Interfacial solar vapor generation not only has a thermodynamic advantage of a high energy transfer efficiency but also possesses a kinetic advantage of a fast response. It has been investigated that in an interfacial solar evaporation system, the response time is directly proportional to the thermal mass,[52] as can be described in eq 6, $t_{T_1,V}$ and $t_{T1,I}$ represent the time interval of the temperature rising from ambient temperature to T_1 of a volumetric heating device and an interfacial heating device respectively, and V_w and V_v represent the volume of water (thermal mass) and steam, respectively. It is clear that the due to the reduced thermal mass, the interfacial heating system has a better performance of response speed. Even as the volume ratio

https://dx.doi.org/10.1021/accountsmr.0c00104
Acc. Mater. Res. XXXX, XXX, XXX−XXX

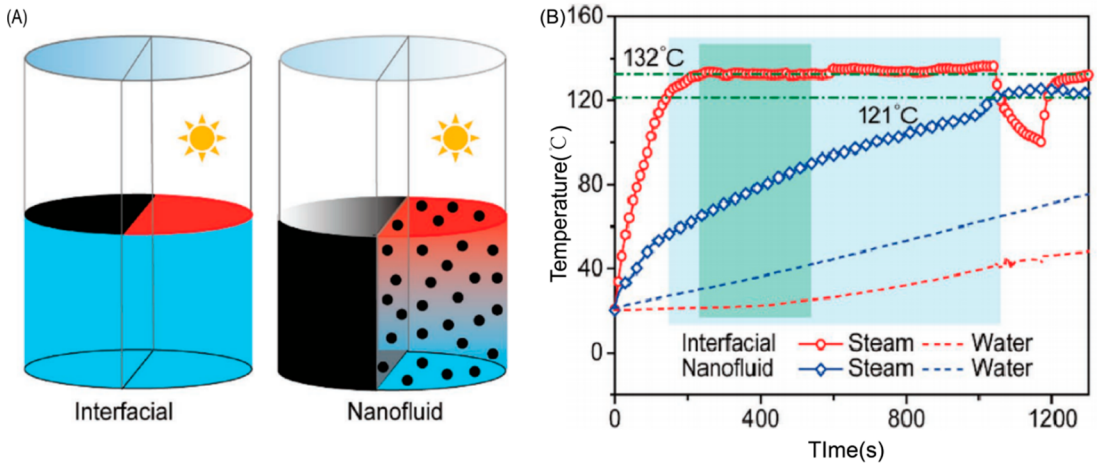

Figure 6. (A) Schematics of interfacial and volumetric heating (nanofluid as a typical instance) without (left half) and with sunlight (right half). (B) Evolutions of temperatures (steam and water) of interfacial and volumetric (nanofluid) heating over time. The blue and green boxes indicate the sterile regime, namely, over 121 °C for 15 min or over 132 °C for 5 min, respectively. Vessels with the same steam volume are used for fair comparison. Reproduced with permission from ref 53. Copyright 2018 Wiley.

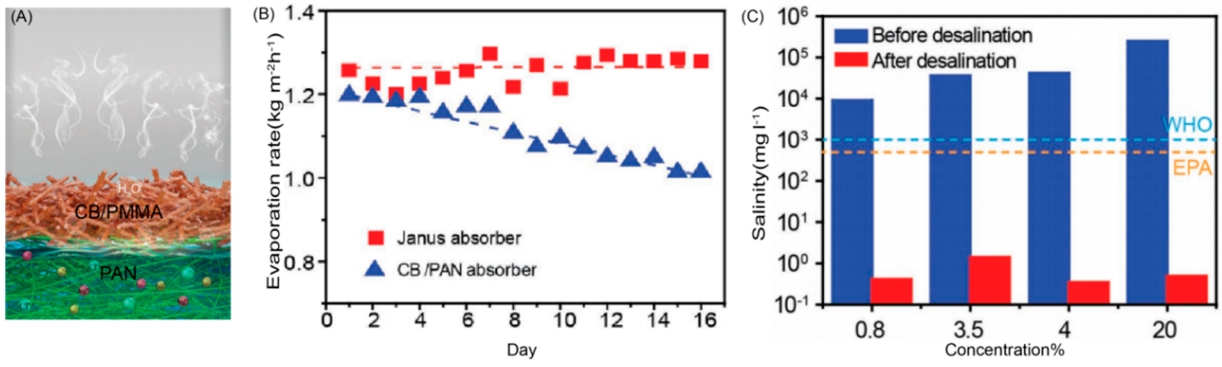

Figure 7. (A) Structures of the Janus absorber for solar desalination. (B) The long-term stability of the Janus absorber and CB/PAN membrane. (C) The measured salinities (the weight percentage of Na^+) of the four simulated seawater samples before and after desalination. Reproduced with permission from ref 47. Copyright 2018 Wiley.

V_w/V_v decreases to 1/5, the intrinsic time interval required by volumetric heating is ~30 times longer than that of interfacial heating.

$$\frac{t_{T_1,V}}{t_{T_1,I}} \approx 1 + 148\frac{V_w}{V_v} \quad (6)$$

In 2017, Li et al. presented an interfacial solar steam generator with superior kinetic performance.[53] Within 3 min, the steam temperature can reach 132 °C under concentrated solar irradiation, which was almost 9 times faster than volumetric type solar heating (Figure 6B). This quick-response and high-temperature steam generation achieved can be attributed to two factors. Interfacial heating localizes the input energy on the top layers of water molecules, which highly reduces the thermal mass compared with a volumetric type heating system. In addition, as bulk water is not heated up in the case of interfacial solar steam generation, the thermal loss is also reduced, which is beneficial for concentrating the absorbed solar energy for high-temperature steam.

3. APPLICATIONS FOR INTERFACIAL SOLAR VAPOR GENERATION

As discussed above, during solar evaporation, vapor is generated, which can be condensed to obtain purified water. Also, as water evaporates, solute in the original water source is left behind, leading to separation of water and solute. In addition, high-temperature steam, as a useful form of energy, can be used for sterilization and/or power generation. Because of the thermodynamic and kinetic advantages of interfacial solar vapor generation listed above, it holds great promise in a broad range of applications, such as desalination, sterilization, power generation, and wastewater treatment.

3.1. Desalination

During solar evaporation, solute will be left behind; therefore, the condensed water will be highly purified, which serves the purpose of desalination. Compared to the concentrations of ions (such as Pb^{2+}, Cr^{2+}, and Cu^{2+}) in seawater, it is found that the concentrations in condensed water can be dramatically reduced by more than 2 orders of magnitude.[34]

However, for traditional solar evaporators used for desalination, as water evaporates, salt will be accumulated on the surface of evaporators, blocking both sunlight absorption and a pathway for vapor escape, resulting in a decline of the vapor generation performance. Therefore, salt accumulation or water fouling issues need to be addressed for stable solar desalination.[46]

In 2018, Xu et al. fabricated a flexible double-layered Janus membrane with excellent salt resistance (Figure 7A).[47] The upper layer is based on hydrophobic poly(methyl methacrylate)

https://dx.doi.org/10.1021/accountsmr.0c00104
Acc. Mater. Res. XXXX, XXX, XXX−XXX

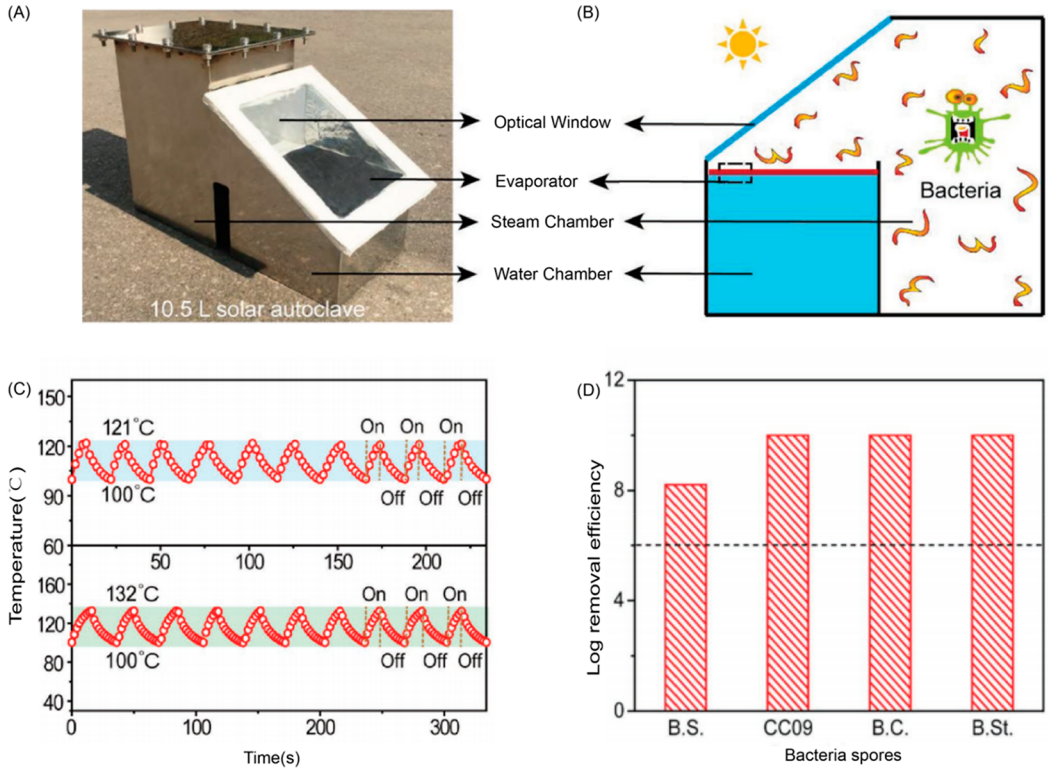

Figure 8. (A) Photograph and (B) a schematic of the interfacial-heating-based solar autoclave. (C) Continuous cycles for the interfacial-heating-based steam generation system. The cycles were obtained by successively turning on (heating) and off (cooling) the light source. The top edge and bottom margin of the box indicate the required sterilizing temperature (121 °C for the blue box and 132 °C for the green box) and the safe temperature to open the sterilization instrument (100 °C), respectively. (D) Inactivation efficiency of bacterial vegetative spores achieved by interfacial-heating-based solar steam sterilization. Reproduced with permission from ref 53. Copyright 2018 Wiley.

(PMMA)/carbon black (CB) NPs, which act as a solar absorber, and the bottom layer composed of hydrophilic polyacrylonitrile (PAN) is used for a water supply. With this Janus design of the upper hydrophobic layer and bottom hydrophilic layer, this solar evaporator can realize excellent resistance to salt when treating seawater, as salt can only be deposited in the bottom hydrophilic PAN layer and be dissolved by a continuous water supply.

Direct solar desalination with a stable water output of 1.3 kg/m^2 h under 1 sun was achieved, and the energy transfer efficiency was calculated to be 72%. During the entire 16-day desalination, the evaporation rate of the as-prepared Janus absorber remained stable at ∼1.3 kg/m^2 h, indicating an excellent salt resistance property, while the regular CB/PAN membrane shows over more than 30% decay in performance (Figure 7B).

The quality of the condensed water was carefully examined. It is found that the salinity is reduced by around 4 orders of magnitude after desalination, meeting the standard by the World Health Organization (WHO) and the US Environmental Protection Agency (Figure 7C).[48]

There are a few other anticlogging designs developed. For example, Kashyap et al. presented an anticlogging structure consisting of a porous polymer skeleton with embedded graphite flakes and carbon fibers.[49] With the help of the geometry of the structure and anticlogging coating, salt will directly deposited at the bottom of the water through the pores rather than accumulating on the absorber. Another floating multilayer solar evaporator was also proposed by Chen's group to overcome the salt-clogging problem.[50] The structure contains three parts: (1) fabric wicks for water pumping; (2) polystyrene foam as insulation layer; and (3) black fabric for solar absorption. During the interfacial evaporation, as the salt concentration of the interfacial region increases, the concentration gradient serves as the driving force of salt diffusion. By taking advantage of the excellent water transporting ability of the wicks and the evaporator, both the water flux and salt flux can undergo adequate transfer and diffusion, dramatically decreasing the salt concentration inside the evaporator.

3.2. Sterilization

As interfacial solar evaporation can generate high-temperature steam in a short period, it is ideal for steam sterilization,[51] in which bacteria can be effectively sterilized by high-temperature steams. A classical steam sterilization process requires a temperature of 121 °C for 15 min or 132 °C for 5 min.[52]

To enable effective, efficient, and high-throughput sterilization, the steam temperature and the response time become essential. In 2018, Li et al. presented an interfacial solar sterilization process based on a cost-effective biomass charcoal-based solar absorber[53] (Figure 8A,B). Because of the kinetic advantage of interfacial solar heating discussed above, the temperature of the steam reaches 121 °C within 122 s, much faster than volumetric heating (over 1040 s) (Figure 8B). In addition, because of the reduced thermal mass, this steam can also be cooled down very quickly. In a commercial autoclave, the cooling process takes as long as 50 min. However, in the interfacial solar sterilization, the cooling procedure only takes approximately 20.2 s, from 132 to 100 °C, which is negligible compared with the duration of the exposure phase (5 min), as shown in Figure 8C.

Therefore, the interfacial solar sterilization process presented is both fast (8.4 min for the full cycle) and energy efficient (100

https://dx.doi.org/10.1021/accountsmr.0c00104
Acc. Mater. Res. XXXX, XXX, XXX−XXX

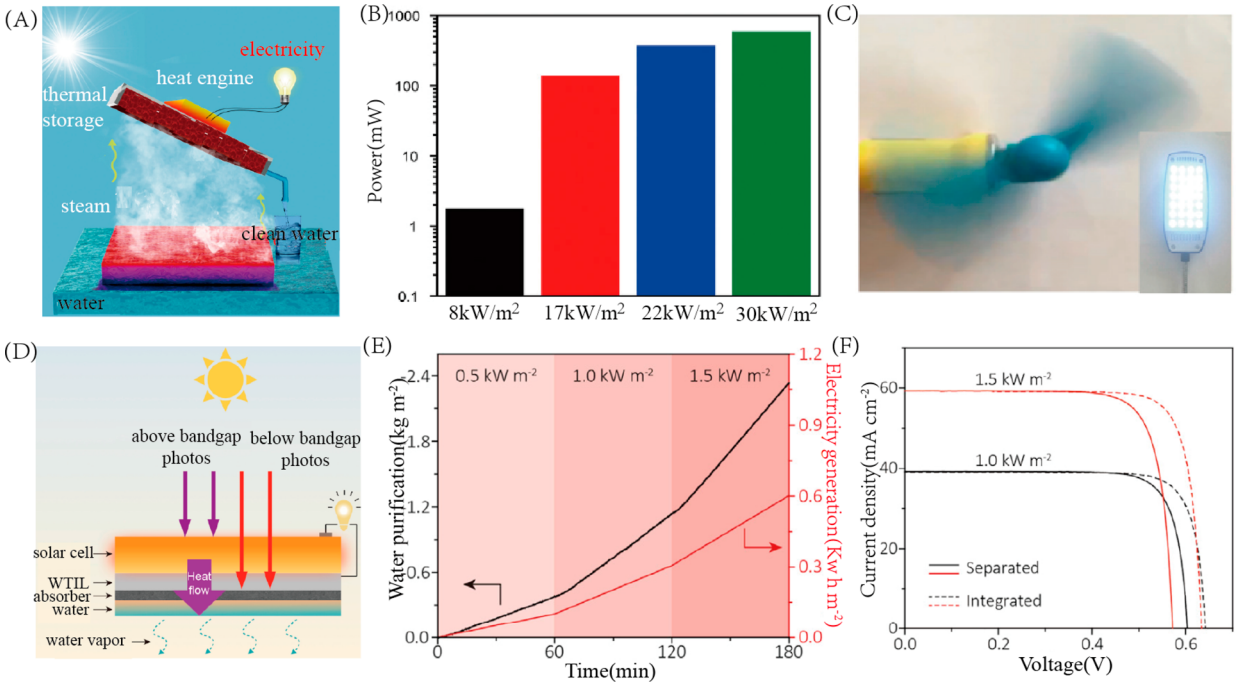

Figure 9. (A) Storage and recycling of interfacial solar steam enthalpy for simultaneous generation of clean water and electricity. (B) Maximum output power of the thermoelectric device under different solar irradiations. (C) Optical image of an operating electric fan and an illuminating light-emitting diode powered by interfacial solar steam generation. Reproduced with permission from ref 58. Copyright 2018 Elsevier. (D) Schematic of the tandem solar electricity−water generator with a synergic effect. (E) Continuous working performances of simultaneous electricity production and water purification under various illumination intensities. (F) Photovoltaic performances of the Si solar cell in separated and integrated systems under illuminations of 1.0 and 1.5 kW m^{-2}. Reproduced with permission from ref 59. Copyright 2020 Elsevier.

J/mL for steam reaching 121 °C), enabling 99.999999% inactivation of the pathogen.

Four kinds of bacterial vegetative cells are used to assess the universal sterilization capability, which can be described by the log removal efficiency, where C_t represents the concentration of surviving microorganisms after the time interval t, and C_0 represents the initial concentration of microorganisms.

$$\mathrm{LRE} = -\log(C_t/C_0) \tag{7}$$

As presented in Figure 8D, for all four different kinds of bacterial vegetative spores, a removal efficiency of over 8 LRE was achieved. This result therefore confirms that interfacial-heating-based solar steam sterilization is effective for inactivation of all vegetative spores and therefore ideal for various sterilization applications.

3.3. Electricity Generation

During the solar steam generation process, the steam generated contains a great amount of energy, called the latent heat of vaporization, which will be completely released during the condensation and typically wasted by dissipating into the environment. It is therefore a natural pathway to explore the reuse of the enthalpy for generating other forms of energy such as electricity.[54]

Several pathways have been proposed to realize simultaneous vapor and electricity generation.[55−57] In 2018, Li et al. proposed an approach to utilize the evaporation for power generation with an energy conversion efficiency over 1% for the first time (Figure 9A).[58] A GO-coated nonwoven fabric was used for solar absorption. Under an illumination intensity of 30 suns, high-temperature steam was produced through interfacial heating and then directly guided into a thermoelectric module. With an evaporation rate of 21.7 kg/m^2 h and a steam temperature of 100 °C, an output power of 574 mW (Figure 9B) and a conversion efficiency of 1.23% were achieved, enough to drive small household appliance such as lamps and portable fans, as shown in Figure 9C. In addition, this device contains a thermal storage ability, enabling a lasting output power even after the light is extinguished.

In 2020, by utilizing the full spectrum of solar irradiance through a monolithic tandem solar electricity−water generator (Figure 9D) for the first time, Ning et al. realized water generation and electricity output simultaneously.[59] The device consists of two parts: a top infrared-transparent photovoltaic device and a bottom solar water purifier. During its working process, the above-bandgap photons are absorbed by the top layer to generate photocurrent, while the below-bandgap photons are absorbed by the reduced graphene oxide membrane to generate heat for interfacial solar vapor generation. With the help of a well-designed water-proof thermal interconnecting layer, all of the components can work synergistically, achieving an power output of 204W/m^2 and a water generation of 0.8 kg/m^2 h(Figure 9E,F).There are several other approaches to generate electricity out of evaporation. One notable example is a phenomenon described as "hydrovoltaic" pioneered by Guo et al.[60] It was found that natural water evaporation from the surface of nanostructured carbon coatings could generate electricity with a voltage of up to 1 V lasting for more than 480 h.[54] Another pathway is to take advantage of salinity gradient as a result of evaporation.[55] As evaporation progresses, the salinity gradient from the evaporation surface to the bulk water keeps increasing, inducing directional ion movement and generating an electrical power of approximately 1 W/m^2. In addition, the piezoelectric effect can also be used for electricity. For example, a piezoelectric material, such as a thin PVDF film, can be used to condense the

https://dx.doi.org/10.1021/accountsmr.0c00104
Acc. Mater. Res. XXXX, XXX, XXX−XXX

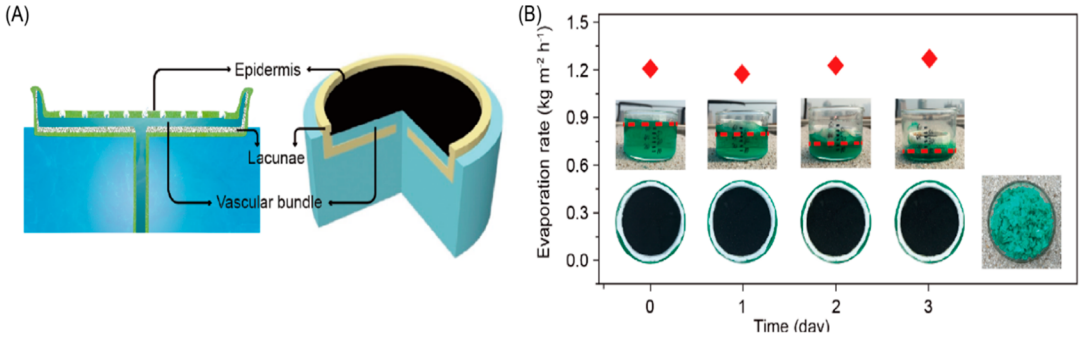

Figure 10. (A) Water lily and water-lily-inspired design for solar vapor generation. (B) Completed separation of water and solute after stable and efficient solar evaporation with the water-lily-inspired evaporator. Reproduced with permission from ref 64. Copyright 2019 The American Association for the Advancement of Science.

vapor.[56] As the condensed water droplets attach to one side of the PVDF film, they will cause stress strong enough to generate electricity as a result of the piezoelectric effect.

3.4. Wastewater Disposal

The alarming issue of water pollution not only exposes the ecosystem to an unprecedented threat but also puts additional stress on the global clean water supply. Interfacial solar vapor generation with a high water evaporation rate provides an alternative avenue to address this crucial issue.

Zero liquid discharge, completed separation of water and solute, has been long pursued as the ultimate goal of wastewater treatment.[61] However, the bottleneck to reach zero liquid discharge is the lack of viable techniques to treat high-salinity brine (>7%). For mainstream technologies like a filtration membrane, energy consumption is significantly increased, and the lifetime is shortened to less than 2 years because of the excessive fouling when treating high-salinity brine.[62,63]

In a recent work, inspired by the elegant transportation system of the water lily, Xu et al. developed a hierarchical antifouling solar evaporator (Figure 10A).[64] The key feature of this structure is that it consists of two layers—a top hydrophobic solar absorber and a bottom stand, which allow a thin water layer sandwiched between the top absorber and bottom stand to be formed during the evaporation process. Unlike most of the interfacial solar evaporators, the thin water layer is formed beneath the absorber rather than within it, effectively preventing the accumulation of salt on the absorber's surface, enabling efficient interfacial vapor generation as well as downward excretion of salt/solute in the 1D channel. As a result, stable and efficient (~80% solar-to-vapor efficiency) evaporation is achieved even when treating high-salinity brine (10 wt %) and wastewater containing heavy metal ions (30 wt %). More strikingly, complete separation of the water and solute is achieved without any salt accumulation on the surface of the evaporator (Figure 10B).

It indicates that interfacial solar evaporation can serve as a viable evaporative technology for wastewater treatment, particularly in these blank areas that have not been covered by the existing technologies.[65,66]

4. CONCLUSION AND OUTLOOK

As shown above, the past few years have witnessed exciting progress in the field of interfacial solar vapor generation, with over 80% efficiency achieved under normal working conditions, through elegant photonic, thermal, and water path designs. The technique also shows unique thermodynamic and kinetic advantages when applied to various fields such as desalination, wastewater treatment, sterilization, and electricity generation. Despite tremendous progress, there are still fundamental questions and technical challenges that need to be addressed.

From the fundamental perspective, it is often a great surprise how limited our knowledge of water and its evaporative behavior is. The microscopic energy transformation, vapor diffusion kinetics at the interface, and tuning of enthalpy remain largely unclear. It is therefore very desirable to develop an advanced technique to observe and characterize the behavior of water particularly within a confined space and investigate the thermodynamic and kinetic processes with high time and spatial resolution.

For interfacial solar vapor generation to make a significant impact at large scale, it is important to pursue a high evaporation rate, combining the other forms of energy in nature. Also for desalination or applications requiring water recovery, it becomes critical to develop advanced condensation technologies to achieve a high collection rate of water. Besides high efficiency and fast response, a low cost and long-term stability are also critical to enable large-scale applications.

From the technical aspect, with the rapid development of materials and devices, the potential applications based on an interfacial photothermal effect can be well-extended.[67−70] For example, one main challenge for high-temperature thermal catalysis is the huge energy consumption, which greatly hinders its industrial development. However, one prominent advantage of interfacial photothermal is the highly localized heating effect without extra energy input, providing a promising way for thermal catalysis. Furthermore, with proper design of evaporators, high-temperature steam can be obtained through concentrated solar light, which can be used in various fields such as disinfection and multieffect distilliation.

Combining solar energy and a water source, the two most abundant resources on earth, used in an efficient way, it is expected that this technique of interfacial solar vapor generation with unique thermodynamic and kinetic advantages can function synergistically with other solar energy devices and water treatment technologies toward a sustainable future.

AUTHOR INFORMATION

Corresponding Author

Jia Zhu − *National Laboratory of Solid State Microstructures, College of Engineering and Applied Sciences, Jiangsu Key Laboratory of Artificial Functional Materials, Nanjing University, Nanjing 210093, P. R. China;* orcid.org/0000-0002-2871-4369; Email: jiazhu@nju.edu.cn

https://dx.doi.org/10.1021/accountsmr.0c00104
Acc. Mater. Res. XXXX, XXX, XXX−XXX

Authors

Xinzhe Min − *National Laboratory of Solid State Microstructures, College of Engineering and Applied Sciences, Jiangsu Key Laboratory of Artificial Functional Materials, Nanjing University, Nanjing 210093, P. R. China*

Bin Zhu − *National Laboratory of Solid State Microstructures, College of Engineering and Applied Sciences, Jiangsu Key Laboratory of Artificial Functional Materials, Nanjing University, Nanjing 210093, P. R. China*

Bo Li − *National Laboratory of Solid State Microstructures, College of Engineering and Applied Sciences, Jiangsu Key Laboratory of Artificial Functional Materials, Nanjing University, Nanjing 210093, P. R. China*

Jinlei Li − *National Laboratory of Solid State Microstructures, College of Engineering and Applied Sciences, Jiangsu Key Laboratory of Artificial Functional Materials, Nanjing University, Nanjing 210093, P. R. China*

Complete contact information is available at: https://pubs.acs.org/10.1021/accountsmr.0c00104

Author Contributions

†X.M., B.Z., and B.L. contributed equally to this work.

Notes

The authors declare no competing financial interest.

Biographies

Xinzhe Min received his B.S. degree from Huazhong University of Science and Technology in 2016 and his M.S. degree from Nanjing University in 2019 under the supervision of Prof. Jia Zhu. His current research interest is photothermal conversion and radiative cooling.

Bin Zhu is an associate professor at College of Engineering and Applied Science, Nanjing University, China. He received his B.S. degree in materials physics from Nanjing University in 2013 and his Ph.D. in Materials Science and Engineering from Nanjing University in 2018. His research interests focus on nanomaterials for energy and environment.

Bo Li received his B.E. degree from Nanjing University of Posts and Telecommunications in 2018. He joined Prof. Jia Zhu's group at Nanjing University to pursue his M.S. degree. His current research interests focus on the application of graphene oxide membrane in water treatment.

Jinlei Li received his B.S. degree from Central South University in 2015 and his M.S. degree from Nanjing University in 2018 under the supervision of Prof. Jia Zhu. His current research interest is photothermal conversion.

Jia Zhu is a professor at College of Engineering and Applied Science, Nanjing University, China. He received his Ph.D. degree in Electrical Engineering from Stanford University. Then, he worked as a postdoctoral fellow at University of California, Berkeley and Lawrence Berkeley National Laboratory. His research interest focuses on tailoring nanomaterials for energy and environmental applications.

■ ACKNOWLEDGMENTS

We acknowledge the microfabrication center of the National Laboratory of Solid State Microstructures (NLSSM) for technique support. This work is jointly supported by the National Key Research and Development Program of China (No. 2017YFA0205700), the National Natural Science Foundation of China (Nos. 12022403, 51925204, 11874211, 61735008, 52002168), the Program for Innovative Talents and Entrepreneur in Jiangsu Province, and the Fundamental Research Funds for the Central Universities (Nos. 021314380150, 021314380140).

■ REFERENCES

(1) Lewis, N. S. Research opportunities to advance solar energy utilization. *Science* **2016**, *351*, aad1920.

(2) Tao, P.; Ni, G.; Song, C.; Shang, W.; Wu, J.; Zhu, J.; Chen, G.; Deng, T. Solar-driven interfacial evaporation. *Nature Energy.* **2018**, *3*, 1031−1041.

(3) Li, X.; Ni, G.; Cooper, T.; Xu, N.; Li, J.; Zhou, L.; Hu, X.; Zhu, B.; Yao, P.; Zhu, J. Measuring Conversion Efficiency of Solar Vapor Generation. *Joule.* **2019**, *3*, 1798−1803.

(4) Zarza, E.; Valenzuela, L.; Leon, J.; Hennecke, K.; Eck, M.; Weyers, H.-D.; Eickhoff, M. Direct steam generation in parabolic troughs: Final results and conclusions of the DISS project. *Energy* **2004**, *29*, 635−644.

(5) Tian, Y.; Zhao, C. Y. A review of solar collectors and thermal energy storage in solar thermal applications. *Appl. Energy* **2013**, *104*, 538−553.

https://dx.doi.org/10.1021/accountsmr.0c00104
Acc. Mater. Res. XXXX, XXX, XXX−XXX

(6) Neumann, O.; Urban, A. S.; Day, J.; Lal, S.; Nordlander, P.; Halas, N. J. J. Solar Vapor Generation Enabled by Nanoparticles. *ACS Nano* **2013**, *7*, 42−49.
(7) Ghadimi, A.; Saidur, R.; Metselaar, H. review of nanofluid stability properties and characterization in stationary conditions. *Int. J. Heat Mass Transfer* **2011**, *54*, 4051−4068.
(8) Zhou, L.; Li, X.; Ni, G.; Zhu, S.; Zhu, J. The revival of thermal utilization from the sun: interfacial solar vapor generation. *National Science Review.* **2019**, *6*, 562−578.
(9) Wang, Z.; Liu, Y.; Tao, P.; Shen, Q.; Yi, N.; Zhang, F.; Liu, Q.; Song, C.; Zhang, D.; Shang, W.; Deng, T. Bio-inspired evaporation through plasmonic film of nanoparticles at the air−water interface. *Small* **2014**, *10*, 3234−3239.
(10) Ghasemi, H.; Ni, G.; Marconnet, A. M.; Loomis, J.; Yerci, S.; Miljkovic, N.; Chen, G. Solar steam generation by heat localization. *Nat. Commun.* **2014**, *5*, 4449.
(11) Zeng, Y.; Yao, J.; Horri, B. A.; Wang, K.; Wu, Y.; Li, D.; Wang, H. Solar evaporation enhancement using floating light-absorbing magnetic particles. *Energy Environ. Sci.* **2011**, *4*, 4074−4078.
(12) Ito, Y.; Tanabe, Y.; Han, J.; Fujita, T.; Tanigaki, K.; Chen, M. Multifunctional porous graphene for high-efficiency steam generation by heat localization. *Adv. Mater.* **2015**, *27*, 4302−4307.
(13) Zhou, L.; Tan, Y.; Ji, D.; Zhu, B.; Zhang, P.; Xu, J.; Gan, Q.; Yu, Z.; Zhu, J. Self-assembly of highly efficient, broadband plasmonic absorbers for solar steam generation. *Science Advances.* **2016**, *2*, e1501227−e1501227.
(14) Zhou, L.; Tan, Y.; Wang, J.; Xu, W.; Yuan, Y.; Cai, W.; Zhu, S.; Zhu, J. 3D self-assembly of aluminium nanoparticles for plasmon-enhanced solar desalination. *Nat. Photonics* **2016**, *10*, 393−398.
(15) Li, X.; Xu, W.; Tang, M.; Zhou, L.; Zhu, B.; Zhu, S.; Zhu, J. Graphene oxide-based efficient and scalable solar desalination under one sun with a confined 2D water path. *Proc. Natl. Acad. Sci. U. S. A.* **2016**, *113*, 13953−13958.
(16) Xiao, G.; Wang, X.; Ni, M.; Wang, F.; Zhu, W.; Luo, Z.; Cen, K. A review on solar stills for brine desalination. *Appl. Energy* **2013**, *103*, 642−652.
(17) Zhou, L.; Li, X.; Ni, G.; Zhu, S.; Zhu, J. The revival of thermal utilization from the Sun: interfacial solar vapor generation. *National Science Review.* **2019**, *6*, 562−578.
(18) Chen, C.; Kuang, Y.; Hu, L. Challenges and Opportunities for Solar Evaporation. *Joule.* **2019**, *3*, 683−718.
(19) Zhao, F.; Guo, Y.; Zhou, X.; Shi, W.; Yu, G. Materials for solar-powered water evaporation. *Nature Reviews Materials.* **2020**, *5*, 388−401.
(20) Wang, P. Emerging investigator series: the rise of nano-enabled photothermal materials for water evaporation and clean water production by sunlight. *Environ. Sci.: Nano* **2018**, *5*, 1078−1089.
(21) Gao, M.; Zhu, L.; Peh, C. K.; Ho, G. W. Solar Absorber Material and System Designs for Photothermal Water Vaporization towards Clean Water and Energy Production. *Energy Environ. Sci.* **2019**, *12*, 841−864.
(22) Zhu, L.; Gao, M.; Peh, C. K. N.; Ho, G. W. Recent progress in solar-driven interfacial water evaporation: Advanced designs and applications. *Nano Energy* **2019**, *57*, 507−518.
(23) Deng, Z.; Zhou, J.; Miao, L.; Liu, C.; Peng, Y.; Sun, L.; Tanemura, S. The emergence of solar thermal utilization: solar-driven steam generation. *J. Mater. Chem. A* **2017**, *5*, 7691−7709.
(24) Wang, J.; Li, Y.; Deng, L.; Wei, N.; Weng, Y.; Dong, S.; Qi, D.; Qiu, J.; Chen, X.; Wu, T. High-Performance Photothermal Conversion of Narrow-Bandgap Ti_2O_3 Nanoparticles. *Adv. Mater.* **2017**, *29*, 1603730.
(25) Zhou, X.; Zhao, F.; Guo, Y.; Zhang, Y.; Yu, G. A hydrogel-based antifouling solar evaporator for highly efficient water desalination. *Energy Environ. Sci.* **2018**, *11*, 1985−1992.
(26) Wang, X.; Liu, Q.; Wu, S.; Xu, B.; Xu, H. Multilayer polypyrrole nanosheets with self-Organized surface structures for flexible and efficient solar-thermal energy conversion. *Adv. Mater.* **2019**, *31*, 1807716.
(27) Yang, y.; Zhao, R.; Zhang, T.; Zhao, K.; Xiao, P.; Ma, Y.; Ajayan, M.; Shi, G.; Chen, Y. Graphene-Based Standalone Solar Energy Converter for Water Desalination and Purification. *ACS Nano* **2018**, *12*, 829−835.
(28) Zhou, X.; Zhao, F.; Guo, Y.; Rosenberger, B.; Yu, G. Architecting highly hydratable polymer networks to tune the water state for solar water purification. *Science Advances.* **2019**, *5*, eaaw5484.
(29) Zielinski, M. S.; Choi, J.-W.; La Grange, T.; Modestino, M.; Hashemi, S. M. H.; Pu, Y.; Birkhold, S.; Hubbell, J. A.; Psaltis, D. Hollow mesoporous plasmonic nanoshells for enhanced solar vapor generation. *Nano Lett.* **2016**, *16*, 2159−2167.
(30) Li, T.; Liu, H.; Zhao, X.; Chen, G.; Dai, J.; Pastel, G.; Jia, C.; Chen, C.; Hitz, E.; Siddhartha, D.; Yang, R.; Hu, L. Scalable and highly efficient mesoporous wood-based solar steam generation device: localized Heat, rapid water transport. *Adv. Funct. Mater.* **2018**, *28*, 1707134.
(31) Xu, N.; Hu, X.; Xu, W.; Li, X.; Zhou, L.; Zhu, S.; Zhu, J. Mushrooms as Efficient Solar Steam-Generation Devices. *Adv. Mater.* **2017**, *29*, 1606762.
(32) Zada, I.; Zhang, W.; Sun, P.; Imtiaz, M.; Iqbal, N.; Ghani, U.; Naz, R.; Zhang, Y.; Li, Y.; Gu, J.; Liu, Q.; Pantelic, D.; Jelenkovic, B.; Zhang, D. Superior photothermal black TiO_2 with random size distribution as flexible film for efficient solar steam generation. *Applied Materials Today* **2020**, *20*, 100669.
(33) Wang, Z.; Liu, Y.; Tao, P.; Shen, Q.; Yi, N.; Zhang, F.; Liu, Q.; Song, C.; Zhang, D.; Shang, W.; Deng, T. Bio-inspired evaporation through plasmonic film of nanoparticles at the air-water interface. *Small* **2014**, *10*, 3234−3239.
(34) Chen, C.; Zhou, L.; Yu, J.; Wang, Y.; Nie, S.; Zhu, S.; Zhu, J. Dual functional asymmetric plasmonic structures for solar water purification and pollution detection. *Nano Energy* **2018**, *51*, 451−456.
(35) Chang, C.; Yang, C.; Liu, Y.; Tao, P.; Song, C.; Shang, W.; Wu, J.; Deng, T. Interfaces. Efficient Solar-Thermal Energy Harvest Driven by Interfacial Plasmonic Heating-Assisted Evaporation. *ACS Appl. Mater. Interfaces* **2016**, *8*, 23412.
(36) Guler, U.; Shalaev, V. M.; Boltasseva, A. Nanoparticle plasmonics: going practical with transition metal nitrides. *Mater. Today* **2015**, *18*, 227−237.
(37) Ishii, S.; Sugavaneshwar, R. P.; Nagao, T. Titanium Nitride Nanoparticles as Plasmonic Solar-Heat Transducers. *J. Phys. Chem. C* **2016**, *120*, 2343−2348.
(38) Hu, X.; Xu, W.; Zhou, L.; Tan, Y.; Wang, Y.; Zhu, S.; Zhu, J. Tailoring Graphene Oxide-Based Aerogels for Efficient Solar Steam Generation under One Sun. *Adv. Mater.* **2017**, *29*, 1604031.
(39) Lou, J.; Liu, Y.; Wang, Z.; Zhao, D.; Song, C.; Wu, J.; Dasgupta, N.; Zhang, W.; Zhang, D.; Tao, P.; Shang, W.; Deng, T. Bioinspired Multifunctional Paper-Based RGO Composites for Solar-Driven Clean Water Generation. *ACS Appl. Mater. Interfaces* **2016**, *8*, 14628.
(40) Li, X.; Lin, R.; Ni, G.; Xu, N.; Hu, X.; Zhu, B.; Lv, G.; Li, J.; Zhu, S.; Zhu, J. Three-dimensional artificial transpiration for efficient solar waste-water treatment. *National Science Review.* **2018**, *5*, 70−77.
(41) Shi, Y.; Li, R.; Jin, Y.; Zhuo, S.; Shi, L.; Chang, J.; Hong, S.; Ng, K.-C.; Wang, P. A 3D Photothermal Structure toward Improved Energy Efficiency in Solar Steam Generation. *Joule.* **2018**, *2*, 1171−1186.
(42) Liu, Y.; Yu, S.; Feng, R.; Bernard, A.; Liu, Y.; Zhang, Y.; Duan, H.; Shang, W.; Tao, P.; Song, C.; Deng, T. Bioinspired, reusable, paper-based system for high-performance large-scale evaporation. *Adv. Mater.* **2015**, *27*, 2768−2774.
(43) Li, X.; Li, J.; Lu, J.; Xu, N.; Chen, C.; Min, X.; Zhu, B.; Li, H.; Zhou, L.; Zhu, S.; Zhang, T.; Zhu, J. Enhancement of Interfacial Solar Vapor Generation by Environmental Energy. *Joule.* **2018**, *2*, 1331−1338.
(44) Liu, Z.; Song, H.; Ji, D.; Li, C.; Cheney, A.; Liu, Y.; Zhang, N.; Zeng, X.; Chen, B.; Gao, J.; Li, Y.; Liu, X.; Aga, D.; Jiang, S.; Yu, Z.; Gan, Q. Solar Vapor Generation: Extremely Cost-Effective and Efficient Solar Vapor Generation under Nonconcentrated Illumination Using Thermally Isolated Black Paper. *Glob Chall.* **2017**, *1*, 1600003.
(45) Li, J.; Wang, X.; Lin, Z.; Xu, N.; Li, X.; Liang, J.; Zhao, W.; Lin, R.; Zhu, B.; Liu, G.; Zhou, L.; Zhu, S.; Zhu, J. Over 10 kg m^{-2} h^{-1}

https://dx.doi.org/10.1021/accountsmr.0c00104
Acc. Mater. Res. XXXX, XXX, XXX−XXX

Evaporation Rate Enabled by a 3D Interconnected Porous Carbon Foam. *Joule.* **2020**, *4*, 928−937.
(46) Crawford, S. E.; Hartmann, M. J.; Millstone, J. E. Surface Chemistry-Mediated Near-Infrared Emission of Small Coinage Metal Nanoparticles. *Acc. Chem. Res.* **2019**, *52*, 695−703.
(47) Xu, W.; Hu, X.; Zhuang, S.; Wang, Y.; Li, X.; Zhou, L.; Zhu, S.; Zhu, J. Flexible and Salt Resistant Janus Absorbers by Electrospinning for Stable and Efficient Solar Desalination. *Advanced Energy Materials.* **2018**, *8*, 1702884.
(48) Chaturvedi, S.; Dave, P. Removal of iron for safe drinking water. *Desalination* **2012**, *303*, 1−11.
(49) Kashyap, V.; Al-Bayati, A.; Sajadi, S. M.; Irajizad, P.; Wang, S. H.; Ghasemi, H. A flexible anti-clogging graphite film for scalable solar desalination by heat localization. *J. Mater. Chem. A* **2017**, *5*, 15227−15234.
(50) Ni, G.; Zandavi, S. H.; Javid, S. M.; Boriskina, S. V.; Cooper, T. A.; Chen, G. A salt-rejecting floating solar still for low-cost desalination. *Energy Environ. Sci.* **2018**, *11*, 1510−1519.
(51) Zhang, Y.; Zhao, D.; Yu, F.; Yang, C.; Lou, J.; Liu, Y.; Chen, Y.; Wang, Z.; Tao, P.; Shang, W.; Wu, J.; Song, C.; Deng, T. Floating rGO-based black membranes for solar driven sterilization. *Nanoscale* **2017**, *9*, 19384−19389.
(52) Neumann, O.; Neumann, A. D.; Tian, S.; Thibodeaux, C.; Shubhankar, S.; Muller, J.; Silva, E.; Alabastri, A.; Bishnoi, S. W.; Nordlander, P.; Halas, N. J. Combining Solar Steam Processing and Solar Distillation for Fully Off-Grid Production of Cellulosic Bioethanol. *ACS Energy Letters.* **2017**, *2*, 8−13.
(53) Li, J.; Du, M.; Lv, G.; Zhou, L.; Li, X.; Bertoluzzi, L.; Liu, C.; Zhu, S.; Zhu, J. Interfacial Solar Steam Generation Enables Fast-Responsive, Energy-Efficient, and Low-Cost Off-Grid Sterilization. *Adv. Mater.* **2018**, *30*, 1805159.
(54) Chen, X.; Goodnight, D.; Gao, Z.; Cavusoglu, A. H.; Sabharwal, N.; DeLay, M.; Driks, A.; Sahin, O. Scaling up nanoscale water-driven energy conversion into evaporation-driven engines and generators. *Nat. Commun.* **2015**, *6*, 7346−7352.
(55) Xue, G.; Xu, Y.; Ding, T.; Li, J.; Yin, J.; Fei, W.; Cao, Y.; Yu, J.; Yuan, L.; Gong, L.; Chen, J.; Deng, S.; Zhou, J.; Guo, W. Water-evaporation-induced electricity with nanostructured carbon materials. *Nat. Nanotechnol.* **2017**, *12*, 317−321.
(56) Yang, P.; Liu, K.; Chen, Q.; Li, J.; Duan, J.; Xue, G.; Xu, Z.; Xie, W.; Zhou, J. Solar-driven simultaneous steam production and electricity generation from salinity. *Energy Environ. Sci.* **2017**, *10*, 1923−1927.
(57) Zhu, L.; Gao, M.; Peh, C. K. N.; Wang, X.; Ho, G. W. Self-Contained Monolithic Carbon Sponges for Solar-Driven Interfacial Water Evaporation Distillation and Electricity Generation. *Advanced Energy Materials.* **2018**, *8*, 1702149.
(58) Li, X.; Min, X.; Li, J.; Xu, N.; Zhu, P.; Zhu, B.; Zhu, S.; Zhu, J. Storage and Recycling of Interfacial Solar Steam Enthalpy. *Joule.* **2018**, *2*, 2477−2484.
(59) Xu, N.; Zhu, P.; Sheng, Y.; Zhou, L.; Li, X.; Tan, H.; Zhu, S.; Zhu, J. Synergistic Tandem Solar Electricity-Water Generators. *Joule.* **2020**, *4*, 347−358.
(60) Zhang, Z.; Li, X.; Yin, J.; Xu, Y.; Fei, W.; Xue, M.; Wang, Q.; Zhou, J.; Guo, W. Emerging hydrovoltaic technology. *Nat. Nanotechnol.* **2018**, *13*, 1109−1119.
(61) Shi, Y.; Zhang, C.; Li, R.; Zhuo, S.; Jin, Y.; Shi, L.; Hong, S.; Chang, J.; Ong, C.; Wang, P. Solar Evaporator with Controlled Salt Precipitation for Zero Liquid Discharge Desalination. *Environ. Sci. Technol.* **2018**, *52*, 11822−11830.
(62) Tong, T.; Elimelech, M. The Global Rise of Zero Liquid Discharge for Wastewater Management: Drivers, Technologies, and Future Directions. *Environ. Sci. Technol.* **2016**, *50* (13), 6846−6855.
(63) Werber, J.; Osuji, C.; Elimelech, M. Materials for next-generation desalination and water purification membranes. *Nature Reviews Materials.* **2016**, *1*, 16018.
(64) Xu, N.; Li, J.; Wang, Y.; Fang, C.; Li, X.; Wang, Y.; Zhou, L.; Zhu, B.; Wu, Z.; Zhu, S.; Zhu, J. A water-lily-inspired hierarchical design for stable and efficient solar evaporation of high salinity brine. *Sci Adv.* **2019**, *5* (7), eeaw7013.
(65) Dongare, P. D.; Alabastri, A.; Pedersen, S.; Zodrow, K. R.; Hogan, N. J.; Neumann, O.; Wu, J.; Wang, T.; Deshmukh, A.; Elimelech, M.; Li, Q.; Nordlander, P.; Halas, N. J. Nanophotonics-enabled solar membrane distillation for off-grid water purification. *Proc. Natl. Acad. Sci. U. S. A.* **2017**, *114*, 6936−6941.
(66) Higgins, M.W.; Shakeel Rahmaan, A.; Devarapalli, R. R.; Shelke, M. V.; Jha, N. Carbon fabric based solar steam generation for waste water treatment. *Sol. Energy* **2018**, *159*, 800−810.
(67) Gao, M.; Peh, C. K.; Zhu, L.; Yilmaz, G.; Ho, G. W. Photothermal catalytic gel featuring spectral and thermal management for parallel freshwater and hydrogen production. *Adv. Energy Mater.* **2020**, *10*, 2000925.
(68) Zhou, Y.; Ding, T.; Gao, M.; Chan, K.; Cheng, Y.; He, J.; Ho, G. W. Controlled heterogeneous water distribution and evaporation towards enhanced photothermal water-electricity-hydrogen production. *Nano Energy* **2020**, *77*, 105102.
(69) Yang, M.-Q.; Tan, C. F.; Lu, W.; Zeng, K.; Ho, G. W. Spectrum tailored defective 2D semiconductor nanosheets aerogel for full-spectrum-driven photothermal water evaporation and photochemical degradation. *Adv. Funct. Mater.* **2020**, *30*, 2004460.
(70) Meng, F. L.; Gao, M.; Ding, T.; Yilmaz, G.; Ong, W. L.; Ho, G. W. Modular deformable steam electricity cogeneration system with photothermal, water, and electrochemical tunable multilayers. *Adv. Funct. Mater.* **2020**, *30*, 2002867.

https://dx.doi.org/10.1021/accountsmr.0c00104
Acc. Mater. Res. XXXX, XXX, XXX−XXX